ACS APPLIED MATERIALS & INTERFACES

Research Article

www.acsami.org

Imaging-Guided Drug Release from Glutathione-Responsive Supramolecular Porphysome Nanovesicles

Xing-Dong Xu,[†] Lingzhi Zhao,[†] Qiuyu Qu,[†] Jin-Gui Wang,[†] Huifang Shi,[†] and Yanli Zhao*[,†,‡]

[†]Division of Chemistry and Biological Chemistry, School of Physical and Mathematical Sciences, Nanyang Technological University, 21 Nanyang Link, 637371, Singapore

[‡]School of Materials Science and Engineering, Nanyang Technological University, 50 Nanyang Avenue, 639798, Singapore

Supporting Information

ABSTRACT: Drug delivery systems that can be employed to load anticancer drugs and release them triggered by a specific stimulus, such as glutathione, are of great importance in cancer therapy. In this study, supramolecular porphysome nanovesicles that were self-assembled by amphiphilic porphyrin derivatives were successfully constructed, mainly driven by the $\pi-\pi$ stacking, hydrogen bonding, and hydrophobic interactions, and were used as carriers of anticancer drugs. The nanovesicles are monodispersed in shape and uniform in size. The drug loading and in vitro drug release investigations indicate that these nanovesicles are able to encapsulate doxorubicin (DOX) to achieve DOX-loaded nanovesicles, and the nanovesicles could particularly release the loaded drug triggered by a high concentration of glutathione (GSH). More importantly, the drug release in cancer cells could be monitored by fluorescent recovery of the porphyrin derivative. Cytotoxicity experiments show that the DOX-loaded nanovesicles possess comparable therapeutic effect to cancer cells as free DOX. This study presents a new strategy in the fabrication of versatile anticancer drug nanocarriers with stimuli-responsive properties. Thus, the porphysome nanovesicles demonstrated here might offer an opportunity to bridge the gap between intelligent drug delivery systems and imaging-guided drug release.

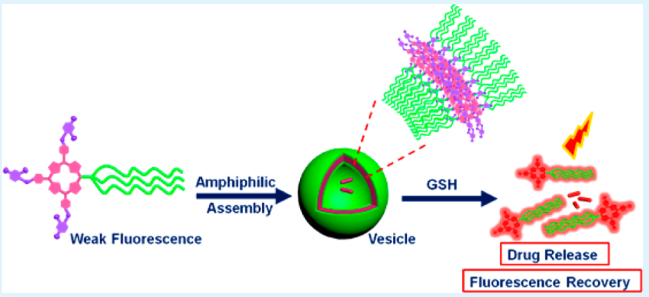

KEYWORDS: *drug delivery, nanovesicles, porphyrin, self-assembly, stimuli-responsive materials*

INTRODUCTION

Nanotechnology has been widely employed in pharmaceutical and biomedical fields,[1,2] which promotes innovative revolution of bioactive drug delivery by developing new drug delivery systems (DDSs).[3,4] These DDSs should be not only constructed with well-defined structures to capture therapeutic drugs but also able to release loaded drugs in response to desired stimuli. The controlled DDSs offer several advantages, such as minimized side effects, better control over drug concentration, low administration frequency, and better drug protection from harsh conditions.[5−7] Numerous systems including decorated liposomes, multifunctional micelles, polymeric hydrogels, and functionalized organic and inorganic nanomaterials have been employed for controlled drug delivery.[8−22] For example, we previously reported a new class of stimuli-responsive mesoporous silica nanoparticles for controlled drug delivery.[12−19] Recently, we studied the fabrication of biocompatible organic nanocarriers through the self-assembly of small organic molecules for efficient drug delivery.[20−22]

Vesicles have been considered as promising delivery vehicles for controlled drug loading and release since their discovery in mid 1960s.[23−29] To effectively achieve controlled release, vesicles should be responsive to external stimuli such as pH change, chemical treatments, enzymatic actions, redox changes, and photoirradiation.[30,31] Given the fact that the concentration of glutathione (GSH) in tumor cells is higher than that in normal cells, GSH has been regarded to be an ideal trigger for redox-sensitive systems to accomplish rapid drug release in cancer cells.[32] To date, several GSH-responsive DDSs have been reported;[33,34] however, the construction of GSH-activated nanovesicles still remains very rare.[35]

As a representative of potentially biocompatible molecules, porphyrins have been extensively investigated on account of their promising applications as photosensitizers in photodynamic therapy.[36−38] The self-assembly behavior and nanostructures of these tetrapyrrole derivatives have attracted a lot of research interests.[39−41] Through reasonable design and modification, such as the introduction of molecular recognition motifs into the porphyrin building blocks, a series of aggregation morphologies including micelles, fibers, and vesicles have been successfully constructed.[42−45] For example, Zheng and co-workers[42] reported the construction of porphysome vesicles by the self-assembly of phospholipid porphyrin conjugates, and the obtained vesicles exhibited high loading capacity, high near-infrared light absorption, and biophotonic properties. To the best of our knowledge, however, stimuli-responsive nanovesicles assembled from

Received: May 27, 2015
Accepted: July 17, 2015
Published: July 17, 2015

DOI: 10.1021/acsami.5b06026
ACS Appl. Mater. Interfaces 2015, 7, 17371−17380

Scheme 1. Chemical Structures and Graphical Representation of GSH-Responsive Porphyrin Derivatives 1 and 2

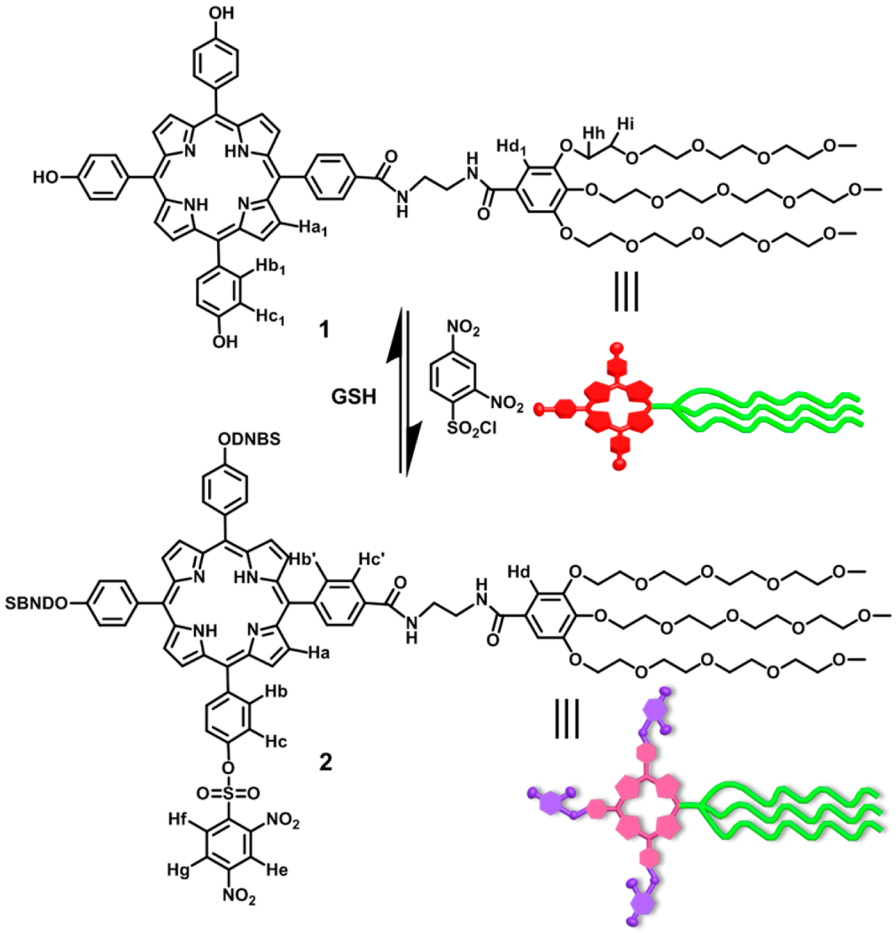

amphiphilic porphyrin derivatives for controlled drug delivery and imaging-guided drug release have not yet been reported.

Imaging-guided drug release in DDSs could provide precise information (a) of when and where the active drugs are delivered and (b) to investigate the accumulation of the drugs at the targeted site in living cells.[46,47] Although several reports on the fabrication of stimuli-responsive DDSs for drug delivery are available in the literature, the development of novel strategies for imaging-guided drug release inside the targeted cells is still in its early stage. Popular strategies include using fluorescent drugs/dyes as model cargos and conjugating nonfluorescent drugs with fluorescent dyes. For example, Kim and Sessler et al.[48,49] have reported GSH-sensitive prodrugs that could image intracellular drug release based on the changes in internal charge transfer (ICT) of fluorophores. Nevertheless, current strategies have some limitations, such as the difficulty in correlating the release of fluorescent model dyes to that of actual drug molecules because most of current drug candidates are nonfluorescent, the usage restriction of fluorescent drugs like doxorubicin (DOX) as cargos, and the possibility of lowering therapeutic efficiency of drugs due to their structural changes required by conjugating with dyes. These challenges in studying the drug release in complex cellular microenvironments require the integration of imaging-guided drug release within stimuli-responsive DDSs.

Herein, we report the synthesis and construction of GSH-responsive porphysome nanovesicles as the delivery system. The porphysome nanovesicles show redox-responsive drug release in the presence of GSH by taking advantage of higher concentration of GSH in cancer cells as compared with normal cells. Recently, 2,4-dinitrobenzenesulfonyl (DNBS) as an efficient recognition site was frequently employed in the construction of thiol-selective probes and reactive oxygen species (ROS) sensors, due to its unique and high reactivity toward thiolate anions such as reduced GSH.[50,51] By conjugating DNBS to a fluorophore, DNBS could often induce the dark state of the fluorophore so that the emission is switched off. The cleavage of DNBS reestablishes the radiative state of the fluorophore, and as a result, the emission is switched on. In this work, a porphyrin chromophore (**1**) was appended to DNBS in order to gain the target compound (**2**), where DNBS "switches off" the fluorescence of the compound **2** (Scheme 1). The DNBS unit can be removed by a well-known thiol-mediated cleavage through nucleophilic aromatic substitution, liberating free porphyrin chromophore with obvious "switched on" fluorescence. During this process, porphysome nanovesicles constructed from the self-assembly of amphiphilic porphyrin compound **2** could be decomposed in a high GSH level, due to the change of molecular structure and hydrophobic-to-hydrophilic transition of the porphyrin fragment. Thus, the present porphysome nanovesicles performs four important roles simultaneously: (i) a nanocarrier for drug delivery, (ii) a GSH-triggered drug release system, (iii) a biocompatible fluorescent chromophore for cell imaging, and (iv) a switchable fluorophore for imaging-guided drug release (Scheme 2).

RESULTS AND DISCUSSION

Synthesis and Characterization. The synthesis of porphyrin derivatives **1** and **2** is outlined in Scheme 1 and Scheme S1 in the

DOI: 10.1021/acsami.5b06026
ACS Appl. Mater. Interfaces 2015, 7, 17371−17380

Scheme 2. Schematic Illustration for the Formation of Supramolecular Porphysome Nanovesicles and Their GSH-Responsive Drug Release and Fluorescence Recovery

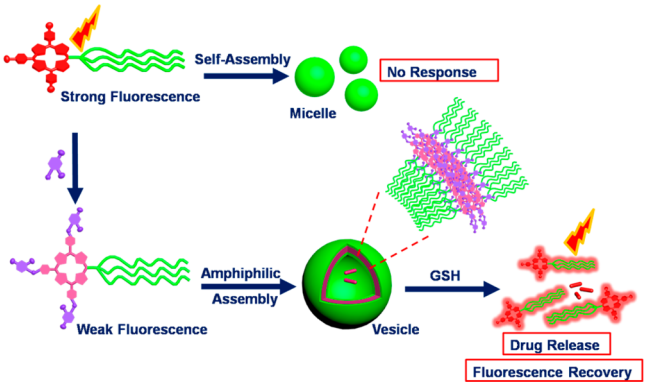

Supporting Information (SI). To synthesize **1**, an intermediate 5-(4-carbomethoxy phenyl)-10,15,20-(4-hydroxy phenyl) porphyrin was first prepared by the condensation of 1 equiv of methyl 4-formylbenzoate and 3 equiv of 4-hydroxybenzaldehyde with pyrrole in propionic acid under refluxing conditions. By using this intermediate compound, two steps of amidation reactions were carried out to get compound **1** in a reasonable yield. The target compound **2** (90% yield) was prepared readily by treating porphyrin derivative **1** with DNBS chloride in the presence of Et_3N in THF (Scheme 1). The molecular structures of compounds **1** and **2** were characterized by using ^1H and ^{13}C NMR spectroscopy and mass spectrometry (refer to the SI for spectroscopic details).

UV−vis absorption spectra of the two compounds in dimethyl sulfoxide (DMSO) are shown in Figure 1 and Figure S2 in the SI. Compound **2** in DMSO exhibits characteristic absorption peaks of the porphyrin unit in the Soret band region at 419 nm and in the Q-band region from 500 to 660 nm. These bands could be assigned to allowed and quasi-allowed $\pi-\pi^*$ transitions, respectively. The spectrum displays monomeric behavior of compound **2** in DMSO, which is evidenced by the single narrow Soret band. The UV−vis spectrum of compound **2** was similar to that of compound **1** (Figure S2 in the SI), indicating that the DNBS unit has no obvious effect on the ground-state property of the porphyrin core. The strong electron-withdrawing 2,4-dinitrobenzenesulfonyl unit was widely employed to quench the fluorescence of various fluorophores (such as porphyrins) by photoinduced electron transfer (PET). Upon excitation at 557 nm, compound **2** exhibits very weak fluorescence emission at 650 nm. Compound **1**, however, shows much stronger fluorescence emission with 7 nm of red shift (Figure 1a), and the emission is 50-fold higher than that of compound **2**. The results clearly indicate that the fluorescence of the porphyrin core in compound **2** was efficiently quenched by the DNBS unit.

Construction of Supramolecular Porphysome Nanovesicles in Water. The nature of multiple intermolecular noncovalent interactions from porphyrin compound **2** stimulated us to investigate its self-assembly behavior in aqueous solution by using scanning electron microscopy (SEM). SEM samples were prepared by depositing the solution of compound **2** onto a SiO_2/Si substrate followed by a slow evaporation in air at room temperature. As demonstrated in Figure 2a, the self-assembled amphiphilic porphyrin **2** exhibits a spherical morphology with a diameter range of 50−200 nm.

In order to further investigate the self-assembly behavior, transmission electron microscopy (TEM) studies were performed. A solution of compound **2** was deposited on copper grids, followed by a slow evaporation in air at room temperature. The existence of spherical entities with an average diameter of ∼100 nm was observed (Figure 2b), which is in good agreement with the SEM measurements. The spherical structure shows a clear contrast between the interior and periphery, matching well with typical characteristics of vesicular structure. The shell thickness of the vesicle-like structure was determined to be ∼8 nm from the TEM image (Figure 2c). Because the extended length of compound **2** calculated by Chem 3D was around 4.5 nm, the vesicle-like structure might possess bilayered compound **2** as the shell (shown in Scheme 2). Different from porphyrin derivative **2**, compound **1** with three hydrophilic phenol OH groups could self-assemble into micelles with an average diameter of 200 nm confirmed by TEM, indicating the significance of molecular structure for the aggregate formation.

Spectroscopic investigation of the porphyrin derivatives in solution was carried out to obtain more information into the self-assembly mode in the formation of vesicle-like structures. The self-assembly behavior of compound **2** was studied by using UV−vis spectroscopy (Figure 1b). UV−vis spectrum of the

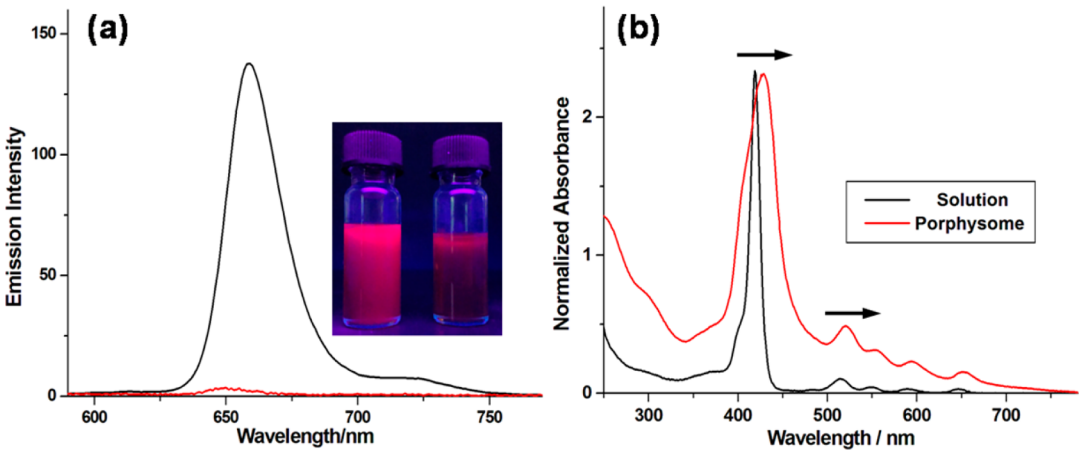

Figure 1. (a) Fluorescence spectra of compounds **1** (black line) and **2** (red line) (both at 0.04 mM) in DMSO excited at 557 nm. Inset shows the emission photos of compounds **1** (left) and **2** (right) upon 365 nm UV lamp irradiation. (b) Normalized UV−vis spectra of compound **2** in DMSO (5.0×10^{-5} M) and in porphysome nanovesicle state.

DOI: 10.1021/acsami.5b06026
ACS Appl. Mater. Interfaces 2015, 7, 17371−17380

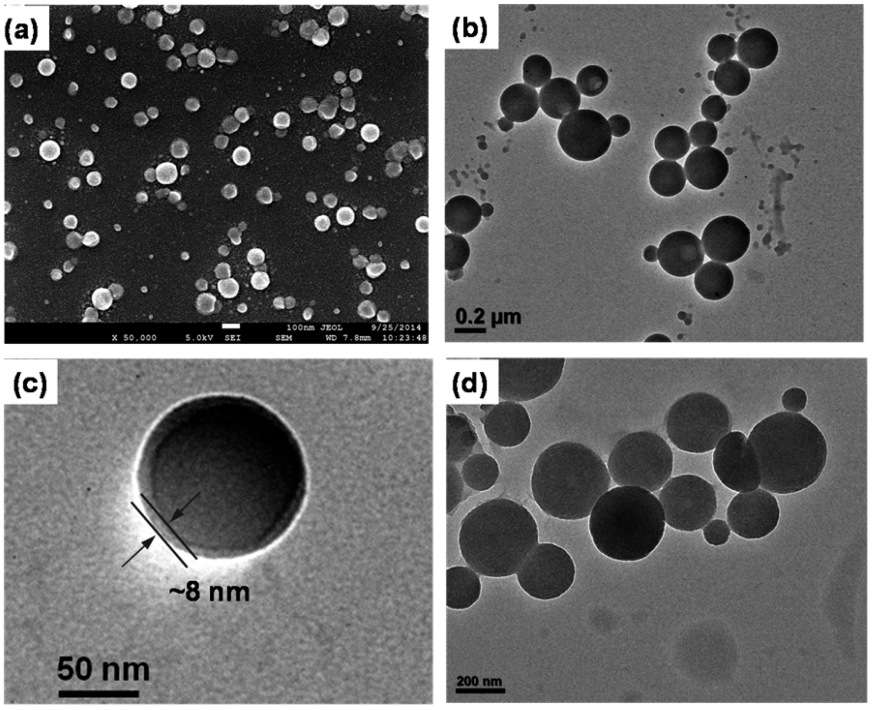

Figure 2. (a) SEM image of nanovesicles self-assembled from compound **2** in aqueous solution. Scale bar is 100 nm. (b) TEM image of nanovesicles self-assembled from compound **2**. Scale bar is 200 nm. (c) Enlarged TEM image. Scale bar is 50 nm. (d) TEM image of aggregates self-assembled from compound **1** in aqueous solution. Scale bar is 200 nm.

porphyrin nanovesicles is significantly different to the spectrum of corresponding compound **2** in solution. As compared to the absorption spectrum of compound **2** in solution, both the Soret and Q bands of the porphyrin core in the nanovesicle state were red-shifted (12 nm for the Soret band and 8.0 nm for the Q-band) and significantly broadened. These observations suggest that *J*-type aggregates were formed in the self-assembly process,[52] which may be facilitated by intermolecular $\pi-\pi$ stacking and hydrophobic interactions.

In addition, the same solution of compound **2** (0.04 mM) showed clear evidence of the Tyndall effect (inset in Figure 3),

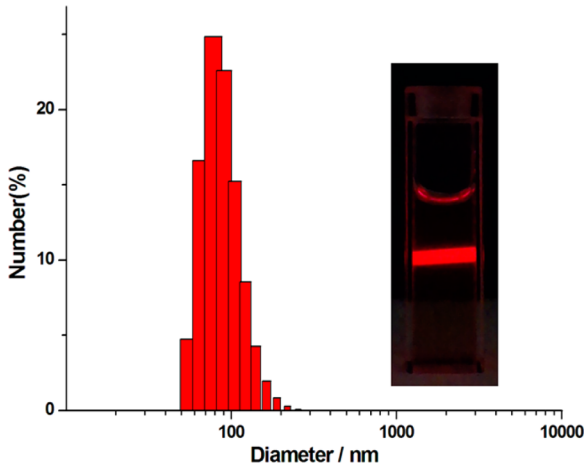

Figure 3. DLS data of the nanovesicles self-assembled from compound **2** (0.04 mM) with an inset showing the Tyndall effect of compound **2**.

demonstrating the formation of nanoscale aggregates.[30] Dynamic laser scattering (DLS) examination reveals that the porphysome nanovesicles have a narrow size distribution, giving an average diameter of 100 nm at a scattering angle of 90° (Figure 3). Furthermore, the plot of optical transmittance versus concentration at 520 nm displays two regimes, exhibiting the critical aggregation concentration (CAC) to be ca. 0.012 mM for compound **2** (Figure S3 in the SI).

In order to investigate the driving forces for the formation of regular aggregates from compound **2**, polarity-dependent ^{1}H NMR spectral experiments in a solvent mixture of acetone-d_6 and D_2O (v/v) were performed (Figure 4). In the polarity-dependent ^{1}H NMR spectra, the increase of polarity from acetone-d_6 to acetone-d_6/D_2O (3/1, v/v) led to slight upfield resonance shifts for the aromatic protons on the DNBS benzyl rings (for example, δ = 9.08 ppm for H_e in acetone-d_6 and δ = 8.97 ppm in acetone-d_6/D_2O 3/1). More importantly, the signals of the pyrrole units in the porphyrin core broadened and even disappeared, while the protons of the benzyl rings split to several peaks due to the strong *J*-aggregation. On the basis of the experimental results obtained, it could be assumed that the formation of regular nanostructures is mainly driven by hydrogen bonding, $\pi-\pi$ stacking, and hydrophobic interactions of porphyrin compound **2**. To further corroborate the mechanism of the nanovesicle formation through the self-assembly of the compound, Fourier transform infrared (FTIR) spectroscopy of the obtained nanovesicles was performed (Figure S4 in the SI). The band centered at 3111 cm^{-1} is a typical character of NH group involved in hydrogen bonding interaction. The presence of the C═O stretching band at 1644 cm^{-1} also evidence the formation of hydrogen-bonded network.

GSH-Responsiveness of Porphysome Nanovesicles. Supramolecular amphiphiles that can form self-assembled nanostructures capable of responding to stimuli are promising candidates for drug delivery applications. Because DNBS could exhibit GSH-responsive properties in aqueous solution,[50,51] it was expected

DOI: 10.1021/acsami.5b06026
ACS Appl. Mater. Interfaces 2015, 7, 17371−17380

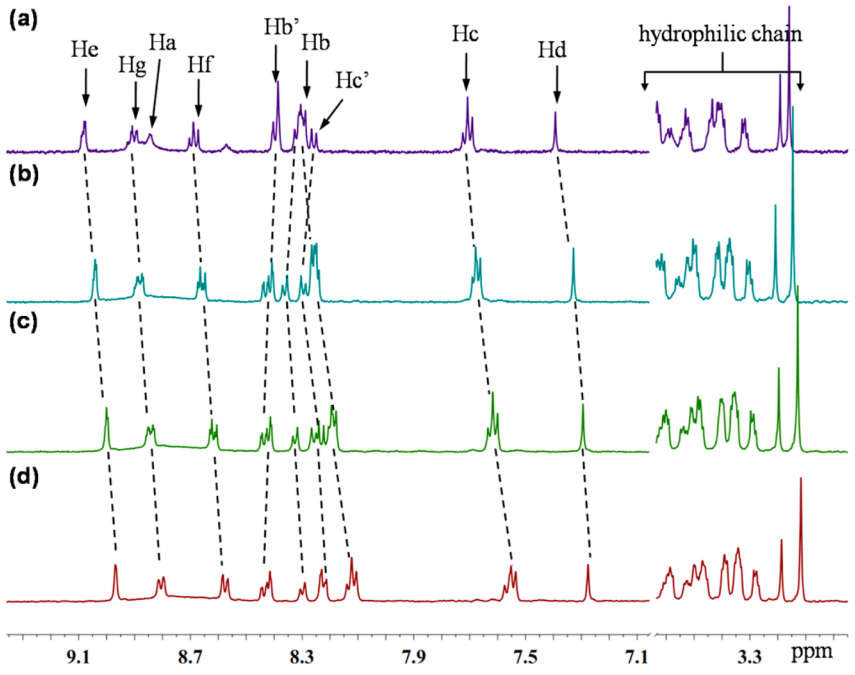

Figure 4. Partial ^{1}H NMR spectra (500 MHz, 298 K) of compound **2** in different volume ratios of acetone-d_6 and D_2O. Acetone-d_6/D_2O = (a) 1:0, (b) 9:1, (c) 4:1, (d) 3:1 (v/v). The proton assignments are indicated in Scheme 1.

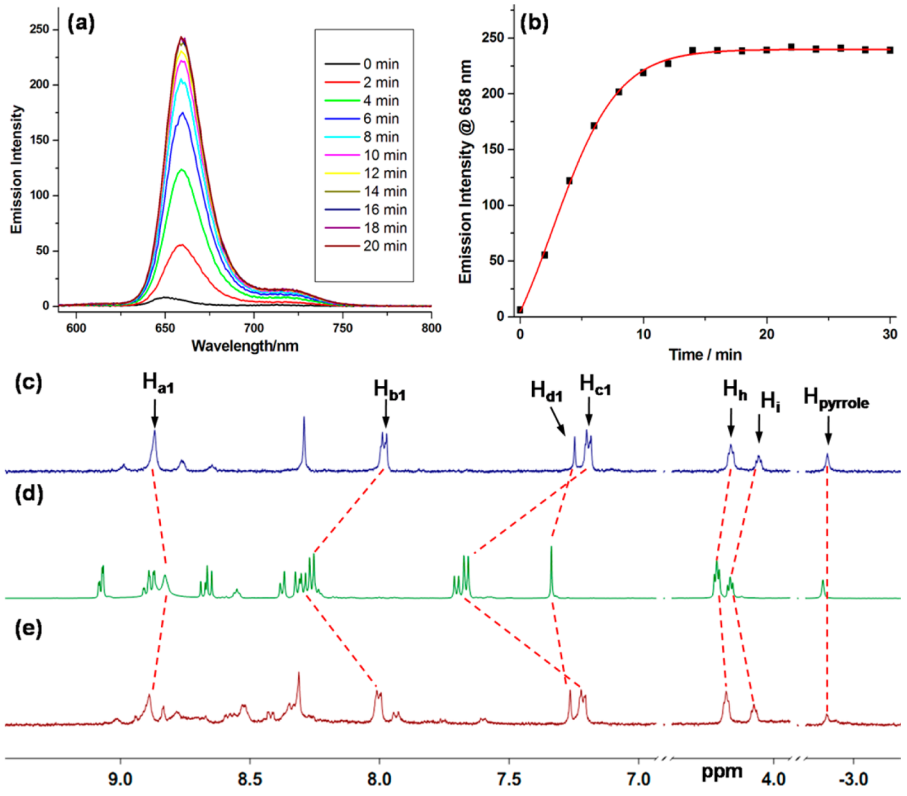

Figure 5. (a) Fluorescence spectra of compound **2** (0.04 mM) in PBS (DMSO/H_2O = 1:4, v/v) at pH 7.4 in the presence of GSH (1.0 mM) with an excitation at 557 nm for different times. (b) Plot showing time-dependent fluorescence intensity changes at 658 nm. Partial ^{1}H NMR spectra (500 MHz, DMSO-d_6, 298 K) of (c) compound **1** and (d) compound **2**. (e) Partial ^{1}H NMR spectrum of compound **2** after the addition of GSH (6 equiv).

that the present nanovesicles constructed from amphiphile porphyrin **2** could show GSH sensitivity.

Redox-responsive property of the porphysome nanovesicles was determined by observing the changes of fluorescence emission in the presence of GSH that mimics the intracellular reducing environment (Figure 5 and Figure S5 in the SI). The addition of increasing concentrations of GSH (0.25−3.0 mM) to a buffer solution of the porphysome induced a recovery of red fluorescence (658 nm) upon excitation at 557 nm. We also recorded time-dependent fluorescence spectra of compound **2**

DOI: 10.1021/acsami.5b06026
ACS Appl. Mater. Interfaces 2015, 7, 17371−17380

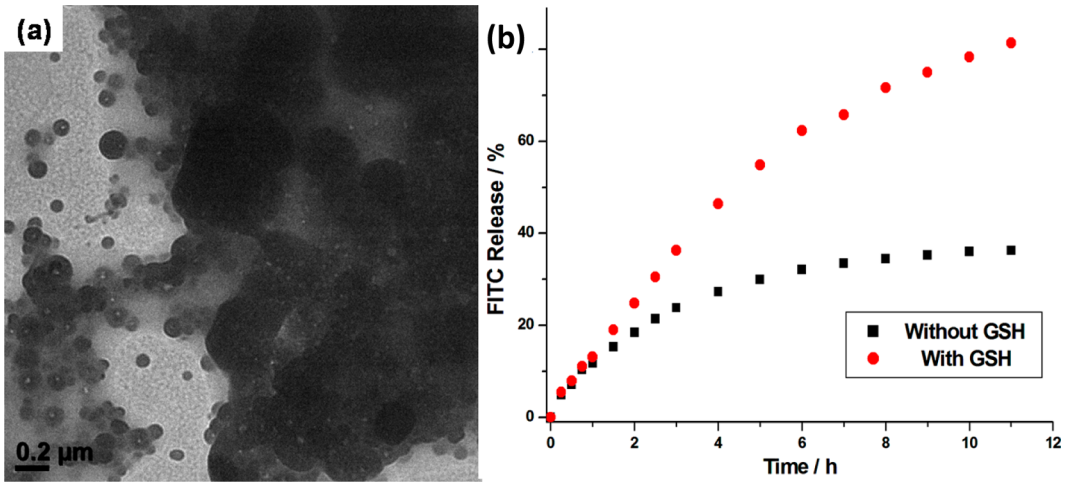

Figure 6. (a) TEM image of the porphysome nanovesicles after the addition of GSH (0.04 mM) overnight. (b) FITC release profiles from FITC-loaded nanovesicles in PBS without and with GSH (1.0 mM) over 11 h.

(0.04 mM) in the presence of GSH (1.0 mM) over 30 min (Figure 5a). Similarly, the fluorescence intensity increased gradually, particularly during the first 15 min. This fluorescent enhancement can be assigned to the separation of the DNBS quencher from the porphyrin core on account of the cleavage of sulfonate ester by GSH. Mass spectrum of compound **2** treated with GSH show a peak at m/z = 247.06 for sulfonate species from the negative model, and another peak at m/z = 1471.80 for phenolic porphyrin species from the positive model (Figure S6 in the SI), further supporting GSH-triggered cleavage mechanism. The final fluorescence intensity was similar to the fluorescence intensity of compound **1** under the same conditions. The cleavage rate was comparable to other systems containing the disulfide bond.[50]

In order to further support the stimuli-responsive dissociation process, in situ ^{1}H NMR investigation of compound **2** in DMSO was carried out (Figure 5). The addition of GSH resulted in the dissociation of the porphyrin core and DNBS group a s detected in ^{1}H NMR studies. For instance, typical proton signals of the porphyrin core in compound **1** displayed an obvious downfield shift after reacting with the DNBS group to form compound **2** (e.g., H_b, δ = 7.98 ppm for compound **1** and δ = 8.26 ppm for compound **2**; H_c, δ = 7.19 ppm for compound **1** and δ = 7.66 ppm for compound **2**), due to strong electron-withdrawing effect of DNBS. Upon adding GSH to compound **2**, the original proton signals in the ^{1}H NMR spectra were restored, indicating the formation of compound **1**. Such NMR signal changes provide direct evidence for stimuli-responsive quantitative reactions of porphyrin compounds. On the basis of these results, redox-responsive behavior of compound **2** in its monomeric state was confirmed.

Furthermore, the disassembly process of nanovesicles induced by GSH was monitored using TEM. GSH (0.04 mM) was added to the porphysome nanovesicle solution (ca. 0.04 mM), where the GSH concentration was comparable to that of porphyrin compound **2** in a 1:1 ratio. After the GSH addition, the TEM image (Figure 6a) shows that the nanovesicles fused together and transformed into irregular morphologies. Moreover, fluorescein isothiocyanate (FITC) was loaded into the nanovesicles, and the release profiles without and with the exposure to GSH in phosphate buffer solution (PBS) are shown in Figure 6b. In this case, 1.0 mM GSH was employed to trigger the release of FITC, a concentration which was similar to the GSH concentration level in cancer cells.[32] The amount of FITC release reached a maximum of 81% with 1.0 mM GSH addition, due to the separation of the porphyrin unit and the DNBS quencher through the cleavage of sulfonate ester linker by GSH. In contrast, FITC-loaded nanovesicles without GSH addition remained relatively stable, and only 36% of FITC was released under the same conditions (Figure S7 in the SI). Relatively slow release kinetics of GSH-responsive nanovesicles is beneficial to avoid the leakage of loaded drugs from the nanovesicles during the transportation, making this type of nanovesicles ideal nanocarriers for drug delivery.

Encapsulation and Imaging-Guided Release. To validate if the GSH-responsive DDSs based on porphysome nanovesicles are also feasible in cancer cells, cervical cancer cells (HeLa cells) were cultured in the presence of such nanovesicles for 24 h. Considering that there is a fluorescence overlap between fluorescent DOX drug and porphyrin compound **1**, hydrophilic fluorescent dyes, 7-hydroxycoumarin and FITC, which show blue and green emission, respectively, were selected to monitor the release process in real time. To prepare dye-loaded nanovesicles, fluorescent dyes were quickly added into freshly prepared nanovesicle solutions, respectively. After standing overnight, unloaded fluorescent dyes were removed by dialysis. In order to identify the intracellular location of released dyes and fluorescence recovery of porphyrin compound, colocalization experiments were performed using confocal laser scanning microscopy (CLSM).

As shown in Figure 7, 7-hydroxycoumarin can be visualized in blue, FITC in green, and porphyrin compound in red. The purple area in the merged image (Figure 7c) implicates the locations where the dye and nanocarriers coexist. In a parallel experiment with FITC, similar to 7-hydroxycoumarin, the merged image shows an intense yellow area (Figure 7f), indicating the locations where FITC and nanocarriers coexist. Therefore, it was concluded that GSH-induced molecular cleavage of compound **2** from dye-loaded nanovesicles occurred in endoplasmic reticulum (ER), leading to the dye release and fluorescence recovery of porphyrin. Such imaging-guided cargo release is consistent with the fluorescence recovery in solution (Figure 5), demonstrating the applicability of the porphysome nanovesicles for imaging-guided drug/dye release in vitro.

DOX Encapsulation and In Vitro Cytotoxicity. DOX, a typical hydrophilic anticancer drug, was selected as a model drug to investigate the encapsulation efficiency of porphysome

DOI: 10.1021/acsami.5b06026
ACS Appl. Mater. Interfaces 2015, 7, 17371−17380

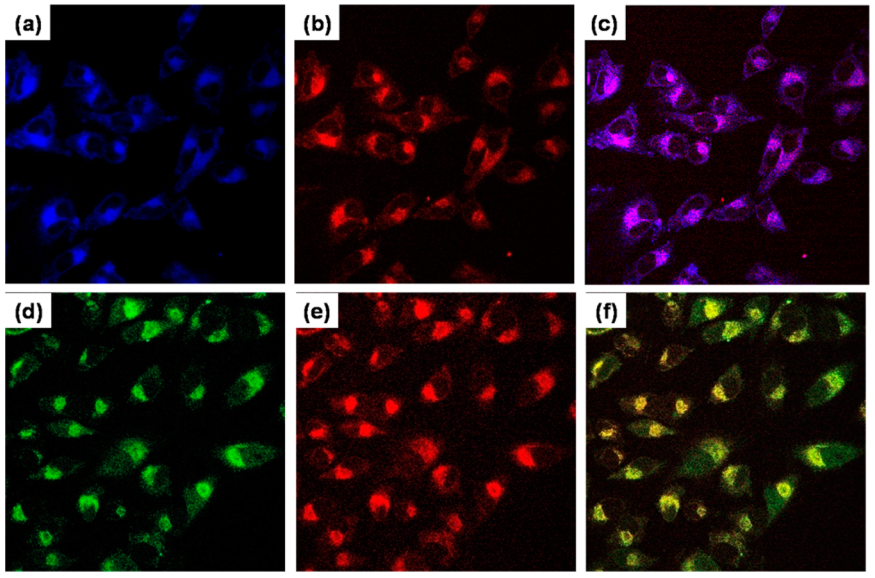

Figure 7. CLSM images of HeLa cells after treated with 7-hydroxycoumarin (4.0 μM) loaded nanovesicles (4.0 μM) for 24 h: (a) 7-hydroxycoumarin channel, (b) porphyrin channel, and (c) merged image of (a) and (b); CLSM images of HeLa cells after treated with FITC (4.0 μM) loaded nanovesicles (4.0 μM) for 24 h: (d) FITC channel, (e) porphyrin channel, and (f) merged image of (d) and (e). Excitation wavelengths (λ_{ex}) at 405 nm for 7-hydroxycoumarin and porphyrin compound, as well as at 488 nm for FITC.

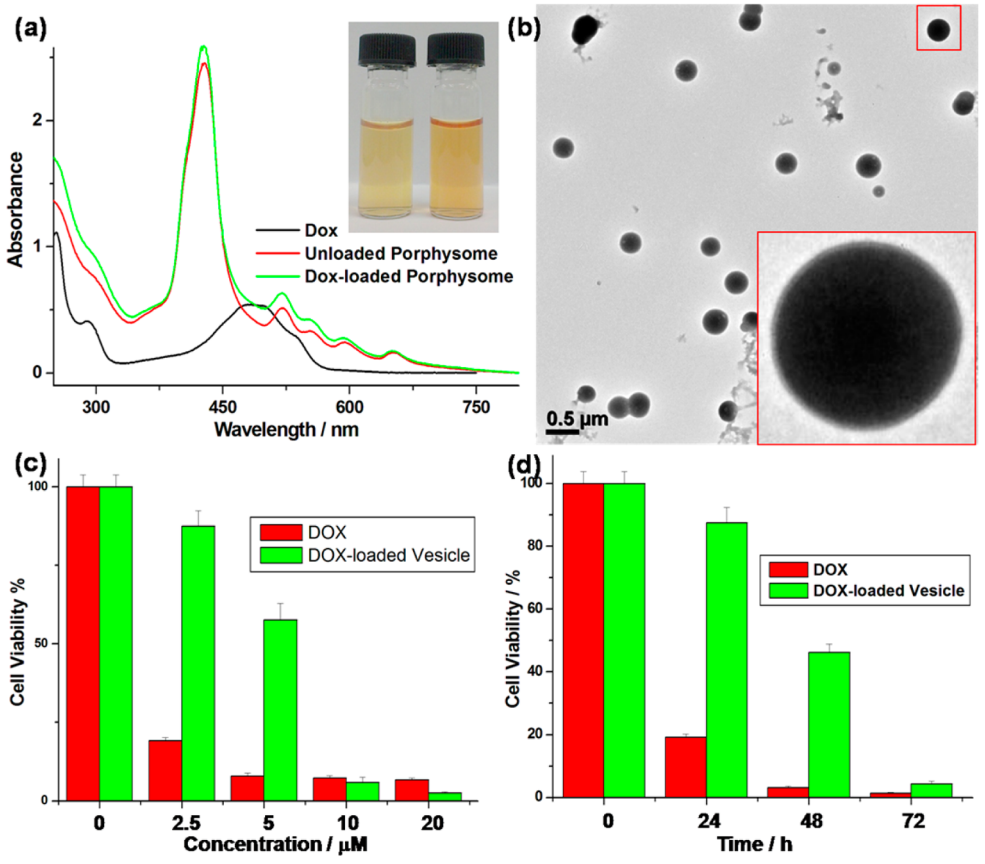

Figure 8. (a) UV−vis absorption spectra of DOX, unloaded nanovesicles, and DOX-loaded nanovesicles in water. Inset shows the color changes of unloaded nanovesicles (left) as compared with DOX-loaded nanovesicles (right). (b) TEM image of DOX-loaded nanovesicles. Inset shows the enlarged area of the TEM image. (c) Anticancer activity of free DOX and DOX-loaded nanovesicles at different concentrations after 24 h of incubation with Hela cells. (d) Anticancer activity of free DOX and DOX-loaded nanovesicles (2.5 μM) in Hela cells under different incubation time.

nanovesicles and the drug release behavior upon the stimulation. As compared with pale yellow vesicular solution, DOX-loaded vesicular solution turned to orange-yellow (Figure 8) after removing unloaded DOX by dialysis, indicating that DOX was successfully loaded into the porphyrin nanovesicles. UV−vis absorption of DOX-loaded vesicular solution became stronger at the range of 420−580 nm than that of unloaded vesicular solution (Figure 8a), because the band from 420 to 580 nm

DOI: 10.1021/acsami.5b06026
ACS Appl. Mater. Interfaces 2015, 7, 17371−17380

represents the characteristic absorption of DOX in aqueous solution. On the basis of the UV−vis absorption spectra, the DOX loading efficiency was calculated to be 6.5%, indicating that the nanovesicles have a reasonable drug-loading capability. In addition, the TEM image (Figure 8b) showed that DOX-loaded nanovesicles were larger in size (320 nm) than unloaded ones (150 nm), confirming that DOX was successfully encapsulated by the nanovesicles. Zeta potential values measured for unloaded and DOX-loaded nanovesicles were around −12.6 and −6.4 mV, respectively (Figure S8 in the SI). The zeta potential difference further indicates the attachment and encapsulation of DOX to nanovesicles, changing their surface charge property.

The cytotoxicity of unloaded porphysome nanovesicles was evaluated by the 3-(4,5-dimethylthiazol-2-yl)-2,5-diphenyltetrazolium bromide (MTT) method against Hela cells. Figure S13 (in the SI) shows the cell viability after 24 and 48 h of incubation with unloaded nanovesicles at a concentration range from 0 to 40 μM. The cell viability remained above 70% when the concentration of unloaded nanovesicles increased to 40 μM after 48 h of incubation. The results are consistent with a previous report that the porphysome can be enzymatically cleaved into pyrroles when incubated with peroxidase and hydrogen peroxide.[15] Consequently, the porphysome nanovesicles with low cytotoxicity are a suitable platform for drug delivery.

The anticancer activity of DOX-loaded nanovesicles with different concentrations was also investigated by MTT assay against Hela cells. As shown in Figure 8c, relative anticancer activity of the free DOX group against cancer cells at low concentration was more efficient than DOX-loaded nanovesicles after 24 h of incubation (e.g., when the concentration was 2.5 μM, the cell viability was 19% for the DOX group and 87% for the DOX-loaded nanovesicle group), which may be due to the fact that DOX can pass through the cell membrane quickly in a simple penetrative diffusion mode. Upon increasing the concentration, the anticancer activity of DOX-loaded nanovesicles tended to be equal with free DOX. For example, the cell viability was 7.3% for free DOX and 5.9% for DOX-loaded nanovesicles under the concentration of 10 μM. Furthermore, the relative viability of Hela cells incubated with free DOX and DOX-loaded nanovesicles under different time was investigated (Figure 8d). The observed results are in accordance with the concentration-dependent experiments (Figure 8c). At the first 24 h, the relative cell viability of DOX-loaded nanovesicles was much higher than free DOX group. However, no obvious difference was observed between the free DOX and the DOX-loaded nanovesicle groups after 72 h of incubation. Because GSH-triggered DOX release takes time (Figure 6), therapeutic efficiency of DOX-loaded nanovesicles could only be comparable to free DOX at a later time. These observations indicate that DOX-loaded nanovesicles could gradually release DOX in vitro to achieve high anticancer efficiency upon time. In addition, the DOX loading by the porphysome nanovesicles did not influence therapeutic effect of DOX to cancer cells. Therefore, such porphysome nanovesicles could be regarded as promising drug delivery vehicles.

CONCLUSIONS

In summary, we have successfully developed a novel amphiphilic porphyrin derivative **2**, which could self-assemble to produce porphysome nanovesicles mainly driven by the $\pi-\pi$ stacking, hydrogen bonding, and hydrophobic interactions. The obtained nanovesicles were monodispersed in shape and uniform in size. By taking advantage of intrinsic supramolecular interactions, the self-assembled nanovesicles were successfully disintegrated due to the separation of the porphyrin unit and the DNBS quencher through the cleavage of sulfonate ester linker by GSH. Meanwhile, the cargo release in cancer cells could be imaging-guided by the fluorescence recovery of the porphyrin derivative. The advantage of this delivery platform is that it could be extended to deliver other fluorescent and nonfluorescent cargoes, since the molecular structure of the porphyrin derivative is responsible for imaging-guided drug release. Drug loading and release experiments have demonstrated that DOX could be successfully loaded into the nanovesicles, and the resultant DOX-loaded nanovesicles showed high GSH responsiveness for controlled DOX release. The cytotoxicity assay of cancer cells has confirmed that DOX-loaded nanovesicles could be effectively internalized by cancer cells, showing therapeutic effects to cancer cells. This study presents a new strategy in the development of versatile drug nanocarriers with stimuli-responsive properties. Thus, the porphysome nanovesicles developed here might open an avenue for the construction of intelligent drug delivery systems with the ability of imaging-guided drug release.

EXPERIMENTAL SECTION

Cell Culture. HeLa cells were cultured in Dulbecco's Modified Eagle's Medium (DMEM) containing 10% fetal bovine serum (FBS) and 2% antibiotics in a humidified atmosphere with 5% CO_2 at 37 °C.

MTT Cytotoxicity Assay. The cytotoxicity of porphysome nanovesicles and DOX-loaded nanovesicles was evaluated by the MTT assay. HeLa cells were seeded into a 96-well plate at a density of 1×10^4 cells/well in DMEM. After 24 h of exposure, the medium in the wells was replaced with fresh medium (100 μL) containing determination substrate (i.e., porphysome nanovesicles or DOX-loaded nanovesicles), with gradually diluted concentrations according to the standard procedure. After incubation for another 24 to 72 h, the medium was removed, and a medium (100 μL) containing MTT (0.5 mg mL^{-1}) was added. After further incubation for 4 h, the medium was replaced with DMSO (100 μL). The plate was gently shaken for 30 min. Then, the absorbance at 560 nm was recorded using a microplate reader (infinite 200 PRO, Tecan). The cell viability related to the control wells that only contain cell culture medium was calculated by $[A]_{test}/[A]_{control}$, where $[A]_{test}$ and $[A]_{control}$ are the average absorption intensities of the test and control samples, respectively.

Confocal Microscopic Images. HeLa cells were seeded in 35 mm plastic-bottomed m-dishes and grown in DMEM for 24 h, and then the cells were treated with dye-loaded nanovesicles (0.04 mM). After another 24 h of incubation, the medium was removed, and the cells were washed with PBS buffer (pH 7.4) three times and fixed with 4.0% formaldehyde at room temperature for 15 min. After 4.0% formaldehyde was removed and the cells were washed with PBS buffer (pH 7.4) three times, the fluorescence images of the cells were captured using a confocal microscope with different channels.

Synthesis of Compound 1. The synthesis of two porphyrin precursors **S1** and **S2** is shown in the SI. 3,4,5-Tris (methyltertraethyleneoxy) benzoic acid (50 mg, 0.067 mmol) and porphyrin compound **S2** (50 mg, 0.067 mmol) were dissolved in dry dimethylformamide (10 mL) under N_2 atmosphere. After the solution was stirred for 10 min, hydroxybenzotriazole (HOBt, 11 mg, 0.081 mmol), *N,N,N′,N′*-tetramethyl-*O*-(1H-benzotriazol-1-yl)uronium hexafluorophosphate (HBTU, 31 mg, 0.081 mmol), and *N,N*-diisopropylethylamine (DIEA, 14 μL, 0.081 mmol) were added to the solution, respectively. The reaction mixture was stirred at room temperature overnight,

DOI: 10.1021/acsami.5b06026
ACS Appl. Mater. Interfaces 2015, 7, 17371−17380

and the solvent was then removed in vacuo. The resultant residue was extracted with ethyl acetate and washed with brine. The organic layers were combined, dried over $MgSO_4$, and concentrated under vacuum. The crude product was purified by column chromatography (acetone/MeOH = 9:1) to afford compound **1** (50 mg, yield 50.5%) as a purple solid. R_f = 0.44 (acetone/MeOH = 9:1), mp = 158.5 °C. ^{1}H NMR (500 MHz, acetone-d_6): δ 8.93 (s, 6H), 8.83 (s, 2H), 8.60 (s, 1H), 8.38 (br, 2H), 8.34 (br, 2H), 8.08−8.05 (m, 6H), 7.36 (s, 2H), 7.31−7.29 (m, 6H), 4.25 (t, J = 9.5 Hz, 4H), 4.19 (t, J = 10.0 Hz, 4H), 3.83−3.81 (m, 6H), 3.76−3.74 (m, 4H), 3.65−3.60 (m, 6H), 3.56−3.48 (m, 14H), 3.42−3.40 (m, 6H), 3.37−3.35 (m, 8H), 3.30−3.28 (m, 4H), 3.22 (s, 3H), 3.16 (s, 6H), 2.60 (s, 2H), 2.14 (s, 2H), −2.70 (s, 2H); ^{13}C NMR (100 MHz, acetone-d_6): δ 168.29, 167.84, 159.50, 153.74, 146.28, 141.97, 136.93, 135.70, 135.64, 133.85, 133.79, 132.60, 131.45, 127.49, 122.28, 121.96, 119.99, 115.38, 108.32, 73.65, 73.06, 72.97, 71.77, 71.66, 71.61, 71.56, 71.51, 71.45, 71.34, 70.79, 70.23, 59.32, 59.26. ESI-MS calcd for $C_{81}H_{94}N_6O_{20}$ $[M + H]^+$, 1471.66; found, 1471.66.

Synthesis of Compound **2**. A solution of 2,4-dinitrobenzenesulfonyl chloride (27.2 mg, 0.100 mmol, 3.0 equiv) in THF (2 mL) was added dropwise into a mixture of porphyrin compound **1** (50 mg, 0.034 mmol) and Et_3N (0.1 mL) in THF (5 mL) under an ice−water bath. The mixture was stirred at room temperature for 30 min. The solvent was then removed in vacuo, and the residue was purified by silica gel column chromatography using acetone/dichloromethane (1:1, v/v) as the eluent to afford compound **2** (66 mg, yield 90.4%) as a purple solid. R_f = 0.54 (acetone/MeOH = 19:1), mp = 106.1 °C. ^{1}H NMR (500 MHz, acetone-d_6): δ 9.08−9.06 (m, 3H), 8.91−8.88 (m, 3H), 8.83 (br, 8H), 8.69−8.65 (m, 3H), 8.55 (s, 1H), 8.37 (d, J = 8.0 Hz, 2H), 8.32−8.25 (m, 8H), 7.71−7.66 (m, 6H), 7.34 (s, 2H), 4.22 (t, J = 9.5 Hz, 4H), 4.17 (t, J = 10.0 Hz, 4H), 3.81−3.79 (m, 6H), 3.76−3.73 (m, 4H), 3.62−3.58 (m, 6H), 3.54−3.46 (m, 14H), 3.40−3.38 (m, 6H), 3.36−3.34 (m, 8H), 3.29−3.27 (m, 4H), 3.21 (s, 3H), 3.14 (s, 6H), 2.60 (s, 2H), 2.14 (s, 2H), −2.88 (s, 2H); ^{13}C NMR (100 MHz, acetone-d_6): δ 168.65, 168.03, 153.59, 153.53, 153.50, 150.78, 150.72, 150.68, 149.77, 149.29, 147.21, 145.95, 143.34, 140.61, 137.32, 135.84, 133.69, 133.64, 132.92, 132.33, 128.82, 127.48, 126.77, 122.43, 122.32, 122.25, 121.46, 120.18, 119.76, 107.87, 73.92, 73.02, 72.96, 71.57, 71.46, 71.45, 71.36, 71.31, 71.26, 71.19, 71.14, 71.02, 70.56, 69.96, 59.55, 59.43. ESI-MS calcd for $C_{99}H_{100}N_{12}O_{38}S_3$ $[M + 2H]^{2+}$, 1081.28; found, 1081.27; $[M + H + Na]^{2+}$, 1092.27; found, 1092.65.

■ ASSOCIATED CONTENT

Supporting Information

Synthesis and characterization details, additional spectroscopic data, SEM and TEM images, in vitro cytotoxicity test, NMR spectra, and MS data. The Supporting Information is available free of charge on the ACS Publications website at DOI: 10.1021/acsami.5b06026.

■ AUTHOR INFORMATION

Corresponding Author

*E-mail: zhaoyanli@ntu.edu.sg.

Notes

The authors declare no competing financial interest.

■ ACKNOWLEDGMENTS

This research is supported by the National Research Foundation (NRF), Prime Minister's Office, Singapore, under its NRF Fellowship (NRF2009NRF-RF001-015) and Campus for Research Excellence and Technological Enterprise (CREATE) Programme-Singapore Peking University Research Centre for a Sustainable Low-Carbon Future, the NTU-A*Star Silicon Technologies Centre of Excellence under program grant no. 11235100003, and the NTU-Northwestern Institute for Nanomedicine.

■ REFERENCES

(1) Lei, J.; Ju, H. Signal Amplification Using Functional Nanomaterials for Biosensing. *Chem. Soc. Rev.* **2012**, *41*, 2122−2134.
(2) Sanchez, C.; Arribart, H.; Madeleine, M.; Guillie, G. Biomimetism and Bioinspiration as Tools for the Design of Innovative Materials and Systems. *Nat. Mater.* **2005**, *4*, 277−288.
(3) Peer, D.; Karp, J. M.; Hong, S.; Farokhzad, O. C.; Margalit, R.; Langer, R. Nanocarriers as an Emerging Platform for Cancer Therapy. *Nat. Nanotechnol.* **2007**, *2*, 751−760.
(4) Kataoka, K.; Harada, A.; Nagasaki, Y. Block Copolymer Micelles for Drug Delivery: Design, Characterization and Biological Significance. *Adv. Drug Delivery Rev.* **2001**, *47*, 113−131.
(5) Mura, S.; Nicolas, J.; Couvreur, P. Stimuli-Responsive Nanocarriers for Drug Delivery. *Nat. Mater.* **2013**, *12*, 991−1003.
(6) Blum, A. P.; Kammeyer, J. K.; Rush, A. M.; Callmann, C. E.; Hahn, M. E.; Gianneschi, N. C. Stimuli-Responsive Nanomaterials for Biomedical Applications. *J. Am. Chem. Soc.* **2015**, *137*, 2140−2154.
(7) Mo, R.; Jiang, T.; DiSanto, R.; Tai, W.; Gu, Z. ATP-Triggered Anticancer Drug Delivery. *Nat. Commun.* **2014**, *5*, 3364−3373.
(8) Yang, Y.; Zhao, Q.; Feng, W.; Li, F. Luminescent Chemodosimeters for Bioimaging. *Chem. Rev.* **2013**, *113*, 192−270.
(9) Babu, S. S.; Praveen, V. K.; Ajayaghosh, A. Functional π-Gelators and Their Applications. *Chem. Rev.* **2014**, *114*, 1973−2129.
(10) Liu, K.; Kang, Y.; Wang, Z.; Zhang, X. Reversible and Adaptive Functional Supramolecular Materials: "Noncovalent Interaction" Matters. *Adv. Mater.* **2013**, *25*, 5530−5548.
(11) Yang, Z. M.; Liang, G. L.; Xu, B. Enzymatic Hydrogelation of Small Molecules. *Acc. Chem. Res.* **2008**, *41*, 315−326.
(12) Ma, X.; Zhao, Y. Biomedical Applications of Supramolecular Systems Based on Host−Guest Interactions. *Chem. Rev.* **2015**, DOI: 10.1021/cr500392w.
(13) Zhao, Y.; Luo, Z.; Li, M.; Qu, Q.; Ma, X.; Yu, S.-H.; Zhao, Y. A Preloaded Amorphous Calcium Carbonate/Doxorubicin@Silica Nanoreactor for pH-Responsive Delivery of an Anticancer Drug. *Angew. Chem., Int. Ed.* **2015**, *54*, 919−922.
(14) Maji, S. K.; Sreejith, S.; Joseph, J.; Lin, M.; He, T.; Tong, Y.; Sun, H.; Yu, S. W.-K.; Zhao, Y. Upconversion Nanoparticles as a Contrast Agent for Photoacoustic Imaging in Live Mice. *Adv. Mater.* **2014**, *26*, 5633−5638.
(15) Luo, Z.; Ding, X.; Hu, Y.; Wu, S.; Xiang, Y.; Zeng, Y.; Zhang, B.; Yan, H.; Zhang, H.; Zhu, L.; Liu, J.; Li, J.; Cai, K.; Zhao, Y. Engineering a Hollow Nanocontainer Platform with Multifunctional Molecular Machines for Tumor-Targeted Therapy *in Vitro* and *in Vivo*. *ACS Nano* **2013**, *7*, 10271−10284.
(16) Zhang, Q.; Wang, X.; Li, P.-Z.; Nguyen, K. T.; Wang, X.-J.; Luo, Z.; Zhang, H.; Tan, N. S.; Zhao, Y. Biocompatible, Uniform, and Redispersible Mesoporous Silica Nanoparticles for Cancer-Targeted Drug Delivery *in Vivo*. *Adv. Funct. Mater.* **2014**, *24*, 2450−2461.
(17) Zhang, Q.; Liu, F.; Nguyen, K. T.; Ma, X.; Wang, X.; Xing, B.; Zhao, Y. Multifunctional Mesoporous Silica Nanoparticles for Cancer-Targeted and Controlled Drug Delivery. *Adv. Funct. Mater.* **2012**, *22*, 5144−5156.
(18) Yan, H.; Teh, C.; Sreejith, S.; Zhu, L.; Kwok, A.; Fang, W.; Ma, X.; Nguyen, K. T.; Korzh, V.; Zhao, Y. Functional Mesoporous Silica Nanoparticles for Photothermal-Controlled Drug Delivery *in Vivo*. *Angew. Chem., Int. Ed.* **2012**, *51*, 8373−8377.
(19) Zhao, Y.-L.; Li, Z.; Kabehie, S.; Botros, Y. Y.; Stoddart, J. F.; Zink, J. I. pH-Operated Nanopistons on the Surfaces of Mesoporous Silica Nanoparticles. *J. Am. Chem. Soc.* **2010**, *132*, 13016−13025.

(20) Jana, A.; Nguyen, K. T.; Li, X.; Zhu, P.; Tan, N. S.; Ågren, H.; Zhao, Y. Perylene-Derived Single-Component Organic Nanoparticles with Tunable Emission: Efficient Anticancer Drug Carriers with Real-Time Monitoring of Drug Release. *ACS Nano* **2014**, *8*, 5939−5952.
(21) Shi, H.; Ma, X.; Zhao, Q.; Liu, B.; Qu, Q.; An, Z.; Zhao, Y.; Huang, W. Ultrasmall Phosphorescent Polymer Dots for Ratiometric Oxygen Sensing and Photodynamic Cancer Therapy. *Adv. Funct. Mater.* **2014**, *24*, 4823−4830.
(22) Zhang, H.; Ma, X.; Nguyen, K. T.; Zhao, Y. Biocompatible Pillararene-Assembly-Based Carriers for Dual Bioimaging. *ACS Nano* **2013**, *7*, 7853−7863.
(23) Du, J. Z.; O'Reilly, R. K. Advances and Challenges in Smart and Functional Polymer Vesicles. *Soft Matter* **2009**, *5*, 3544−3561.
(24) Yang, H.; Yuan, B.; Zhang, X.; Scherman, O. A. Supramolecular Chemistry at Interfaces: Host−Guest Interactions for Fabricating Multifunctional Biointerfaces. *Acc. Chem. Res.* **2014**, *47*, 2106−2115.
(25) Yan, X.; Wang, F.; Zheng, B.; Huang, F. Stimuli-Responsive Supramolecular Polymeric Materials. *Chem. Soc. Rev.* **2012**, *41*, 6042−6065.
(26) Chen, L.-J.; Zhao, G.-Z.; Jiang, B.; Sun, B.; Wang, M.; Xu, L.; He, J.; Abliz, Z.; Tan, H.; Li, X.; Yang, H.-B. Smart Stimuli-Responsive Spherical Nanostructures Constructed from Supramolecular Metallodendrimers *via* Hierarchical Self-Assembly. *J. Am. Chem. Soc.* **2014**, *136*, 5993−6001.
(27) Du, J.; Armes, S. P. pH-Responsive Vesicles Based on a Hydrolytically Self-Cross-Linkable Copolymer. *J. Am. Chem. Soc.* **2005**, *127*, 12800−12801.
(28) Zhang, X.; Rehm, S.; Safont-Sempere, M. M.; Würthner, F. Vesicular Perylene Dye Nanocapsules as Supramolecular Fluorescent pH Sensor Systems. *Nat. Chem.* **2009**, *1*, 623−629.
(29) Chen, S.; Ruan, Y.; Brown, J. D.; Hadad, C. M.; Badjić, D. Recognition Characteristics of an Adaptive Vesicular Assembly of Amphiphilic Baskets for Selective Detection and Mitigation of Toxic Nerve Agents. *J. Am. Chem. Soc.* **2014**, *136*, 17337−17342.
(30) Guo, D.-S.; Wang, K.; Wang, Y.-X.; Liu, Y. Cholinesterase-Responsive Supramolecular Vesicle. *J. Am. Chem. Soc.* **2012**, *134*, 10244−10250.
(31) Cao, Y.; Hu, X.-Y.; Li, Y.; Zou, X.; Xiong, S.; Lin, C.; Shen, Y.-Z.; Wang, L. Multistimuli-Responsive Supramolecular Vesicles Based on Water-Soluble Pillar[6]arene and SAINT Complexation for Controllable Drug Release. *J. Am. Chem. Soc.* **2014**, *136*, 10762−10769.
(32) Meister, A.; Anderson, M. E. Glutathione. *Annu. Rev. Biochem.* **1983**, *52*, 711−760.
(33) Luo, Z.; Cai, K.; Hu, Y.; Zhao, L.; Liu, P.; Duan, L.; Yang, W. Mesoporous Silica Nanoparticles End-Capped with Collagen: Redox-Responsive Nanoreservoirs for Targeted Drug Delivery. *Angew. Chem., Int. Ed.* **2011**, *50*, 640−643.
(34) Wang, X.; Cai, X.; Hu, J.; Shao, N.; Wang, F.; Zhang, Q.; Xiao, J.; Cheng, Y. Glutathione-Triggered "Off-On" Release of Anticancer Drugs from Dendrimer-Encapsulated Gold Nanoparticles. *J. Am. Chem. Soc.* **2013**, *135*, 9805−9810.
(35) Chang, Y.; Yang, K.; Wei, P.; Huang, S.; Pei, Y.; Zhao, W.; Pei, Z. Cationic Vesicles Based on Amphiphilic Pillar[5]arene Capped with Ferrocenium: A Redox-Responsive System for Drug/siRNA Co-Delivery. *Angew. Chem., Int. Ed.* **2014**, *53*, 13126−13130.
(36) Lovell, J. F.; Liu, T. W. B.; Chen, J.; Zheng, G. Activatable Photosensitizers for Imaging and Therapy. *Chem. Rev.* **2010**, *110*, 2839−2857.
(37) Cheng, L.; Wang, C.; Feng, L.; Yang, K.; Liu, Z. Functional Nanomaterials for Phototherapies of Cancer. *Chem. Rev.* **2014**, *114*, 10869−10939.
(38) Lu, K.; He, C.; Lin, W. Nanoscale Metal-Organic Framework for Highly Effective Photodynamic Therapy of Resistant Head and Neck Cancer. *J. Am. Chem. Soc.* **2014**, *136*, 16712−16715.
(39) Li, W.; Aida, T. Dendrimer Porphyrins and Phthalocyanines. *Chem. Rev.* **2009**, *109*, 6047−6076.
(40) Medforth, C. C. J.; Wang, Z.; Martin, K. E.; Song, Y.; Jacobsen, J. L.; Shelnutt, J. A. Self-Assembled Porphyrin Nanostructures. *Chem. Commun.* **2009**, 7261−7277.
(41) Liu, H.; Xu, J.; Li, Y.; Li, Y. Aggregate Nanostructures of Organic Molecular Materials. *Acc. Chem. Res.* **2010**, *43*, 1496−1508.
(42) Lovell, J. F.; Jin, C. S.; Huynh, E.; Jin, H.; Kim, C.; Rubinstein, J. L.; Chan, W. C.W.; Cao, W.; Wang, L. V.; Zheng, G. Porphysome Nanovesicles Generated by Porphyrin Bilayers for Use as Multimodal Biophotonic Contrast Agents. *Nat. Mater.* **2011**, *10*, 324−332.
(43) Ghoroghchian, P. P.; Frail, P. R.; Susumu, K.; Blessington, D.; Brannan, A. K.; Bates, F. S.; Chance, B.; Hammer, D. A.; Therien, M. J. Near-Infrared-Emissive Polymersomes: Self-Assembled Soft Matter for *in Vivo* Optical Imaging. *Proc. Natl. Acad. Sci. U. S. A.* **2005**, *102*, 2922−2927.
(44) Gao, Y.; Zhang, X.; Ma, C.; Li, X.; Jiang, J. Morphology-Controlled Self-Assembled Nanostructures of 5,15-Di[4-(5-Acetylsulfanylpentyloxy)Phenyl]Porphyrin Derivatives. Effect of Metal-Ligand Coordination Bonding on Tuning the Intermolecular Interaction. *J. Am. Chem. Soc.* **2008**, *130*, 17044−17052.
(45) Qiu, Y.; Chen, P.; Liu, M. Evolution of Various Porphyrin Nanostructures *via* an Oil/Aqueous Medium: Controlled Self-Assembly, Further Organization, and Supramolecular Chirality. *J. Am. Chem. Soc.* **2010**, *132*, 9644−9652.
(46) Wu, X.; Sun, X.; Guo, Z.; Tang, J.; Shen, Y.; James, T. D.; Tian, H.; Zhu, W. *In Vivo* and *in Situ* Tracking Cancer Chemotherapy by Highly Photostable NIR Fluorescent Theranostic Prodrug. *J. Am. Chem. Soc.* **2014**, *136*, 3579−3588.
(47) Lai, J.; Shah, B. P.; Garfunkel, E.; Lee, K.-B. Versatile Fluorescence Resonance Energy Transfer-Based Mesoporous Silica Nanoparticles for Real-Time Monitoring of Drug Release. *ACS Nano* **2013**, *7*, 2741−2750.
(48) Lee, M. H.; Han, J. H.; Kwon, P. S.; Bhuniya, S.; Kim, J. Y.; Sessler, J. L.; Kang, C.; Kim, J. S. Hepatocyte-Targeting Single Galactose-Appended Naphthalimide: A Tool for Intracellular Thiol Imaging *in Vivo*. *J. Am. Chem. Soc.* **2012**, *134*, 1316−1322.
(49) Lee, M. H.; Jeon, H. M.; Han, J. H.; Park, N.; Kang, C.; Sessler, J. L.; Kim, J. S. Toward a Chemical Marker for Inflammatory Disease: A Fluorescent Probe for Membrane-Localized Thioredoxin. *J. Am. Chem. Soc.* **2014**, *136*, 8430−8437.
(50) Maeda, H.; Yamamoto, K.; Nomura, Y.; Kohno, I.; Hafsi, L.; Ueda, N.; Yoshida, S.; Fukuda, M.; Fukuyasu, Y.; Yamauchi, Y.; Itoh, N. A Design of Fluorescent Probes for Superoxide Based on a Nonredox Mechanism. *J. Am. Chem. Soc.* **2005**, *127*, 68−69.
(51) He, H.; Lo, P.-C.; Ng, D. K. P. A Glutathione-Activated Phthalocyanine-Based Photosensitizer for Photodynamic Therapy. *Chem. - Eur. J.* **2014**, *20*, 6241−6245.
(52) Xu, X.-D.; Zhang, J.; Chen, L.-J.; Guo, R.; Wang, D.-X.; Yang, H.-B. Design and Synthesis of Branched Platinum-Acetylide Complexes Possessing a Porphyrin Core and Their Self-Assembly Behavior. *Chem. Commun.* **2012**, *48*, 11223−11225.

DOI: 10.1021/acsami.5b06026
ACS Appl. Mater. Interfaces 2015, 7, 17371−17380